Materials Science

Volume 2, Issue 3, 189-202.
DOI: 10.3934/matersci.2015.3.189
Received date 02 April 2015,
Accepted date 25 June 2015,
Published date 01 July 2015

http://www.aimspress.com/

Research article

Simulation and Measurement of Neuroelectrodes´ Characteristics with Integrated High Aspect Ratio Nano Structures

Christoph Nick [1,2], Helmut F. Schlaak [2], and Christiane Thielemann [1,*]

[1] BioMEMS Lab, University of Applied Sciences Aschaffenburg, Wuerzburger Str. 45, 63743 Aschaffenburg, Germany
[2] Institute of Electromechanical Design, Technische Universitaet Darmstadt, Merckstraße 25, 64283 Darmstadt, Germany

* **Correspondence:** Email: christiane.thielemann@h-ab.de; Tel: +49-6021-4206-817; Fax: +49-6021-4206-748.

Abstract: Improving the interface between electrodes and neurons has been the focus of research for the last decade. Neuroelectrodes should show small geometrical surface area and low impedance for measuring and high charge injection capacities for stimulation. Increasing the electrochemically active surface area by using nanoporous electrode material or by integrating nanostructures onto planar electrodes is a common approach to improve this interface. In this paper a simulation approach for neuro electrodes´ characteristics with integrated high aspect ratio nano structures based on a point-contact-model is presented. The results are compared with experimental findings conducted with real nanostructured microelectrodes. In particular, effects of carbon nanotubes and gold nanowires integrated onto microelectrodes are described. Simulated and measured impedance properties are presented and its effects onto the transfer function between the neural membrane potential and the amplifier output signal are studied based on the point-contact-model. Simulations show, in good agreement with experimental results, that electrode impedances can be dramatically reduced by the integration of high aspect ratio nanostructures such as gold nanowires and carbon nanotubes. This lowers thermal noise and improves the signal-to-noise ratio for measuring electrodes. It also may increase the adhesion of cells to the substrate and thus increase measurable signal amplitudes.

Keywords: nanostructured microelectrode; point-contact-model; transfer function; modelling

1. Introduction

The neuron-electrode interface is crucial for many biomedical applications such as [1], retina implants [2], deep brain stimulation [3], closed loop deep brain stimulation [4] or electrocorticography [5]. For electrodes used for electrically stimulating neural tissue a large charge injection capacity is required to guarantee effective stimulation with parameters that are safe for biological tissue. Recording electrodes on the other hand should have low impedance resulting in low thermal noise and a high signal-to-noise ratio (SNR). In both cases the geometrical surface area of neuroelectrodes should be in the dimension of the cell size to guarantee the detection or stimulation of single cell activity. Small electrodes further allow arranging multiple electrodes in a high density array enabling high spatial resolution. One parameter that influences the SNR is the noise of the electrode which is mainly of thermal origin. Consequently noise amplitudes can be reduced by reducing the electrodes´ impedance. Since the impedance is dominantly capacitive this can be achieved by increasing the electrochemical active surface area. A large electrochemical surface area in turn can be achieved by a nanostructured or rough electrode material such as carbon nanotubes [6,7,8], gold nanopillars [9,10], Polypyrrol (PPy) [11] or PEDOT [12]. Although there has been a lot of experimental work on different electrode materials, there is a lack of theoretical models that help to understand and predict the behavior at the interface.

Here we present a surface area based approach to model and simulate the electrode behavior and compare the theoretical expectations with real characteristics of manufactured microelectrodes. As model systems unordered carbon nanotubes and nearly vertically aligned gold nanowires are integrated onto electrodes. In section 2.1 methods of how to integrate the high aspect ratio nano objects onto microelectrodes are presented. In section 2.2 the interface between electrode and neuron is modelled by the well-known point-contact-model. To investigate the influence of biological and electrical parameters on the efficiency of a neuroelectrode, a transfer function describing the interface between neuronal membrane potential and measurable extracellular potential is evolved. From this holistic model a simplified electrode model is derived and the expected properties simulated in Matlab^{TM} (The MathWorks Inc., Natick, USA). Finally these results are compared to real electrodes behavior manufactured by standard microelectromechanical systems (MEMS) technology. Cyclic voltammetry as well as electrochemical impedance spectroscopy are performed on manufactured microelectrodes to investigate the real characteristics and compare it to the simulated data.

2. Materials and Method

2.1. Electrode Design with Integrated Nano Objects

A widely used technique to measure and stimulate neurons in-vitro and in-vivo is an array of microelectrodes (microelectrode array, MEA), suggested in different configurations, e.g. different electrode sizes, distances, arrangements or shapes [13–16]. Here a microelectrode array with an electrode diameter of 30 μm and distance (center to center) of 200 μm is designed. Metallic microelectrodes and circuit paths are structured lithographically and insulated by a thin layer of polyimide or photoresist. Microelectrodes and contact pads are as well opened lithographically and two types of nano objects are integrated subsequently.

2.1.1. Carbon-Nanotubes

Several approaches have been described to manufacture microelectrodes with integrated unordered carbon nanotubes (CNTs) such as chemical vapor depositioning [17], electroplating CNT/polymer composites [18] or transferring CNTs as dispersion [19]. The manufacturing process applied here is described in detail in [20] and schematically depicted in Figure 1. In short, multiwalled carbon nanotubes (Sigma-Aldrich, Taufkirchen, Germany) are transferred in a 1mg/ml-dispersion in N-Methyl-2-pyrrolidon (NMP), dispensed onto a microelectrode array (Figure 1a–b) and the solvent is allowed to evaporate. After removing excessive CNTs with a squeegee, the nano objects remain in the electrode cavities exclusively as depicted in Figure 1c.

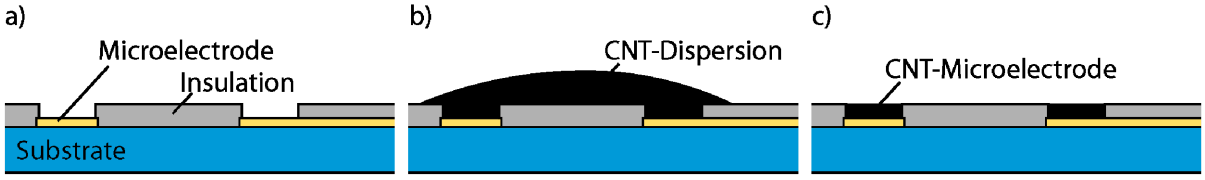

Figure 1. Integration of carbon nanotubes onto microelectrodes. a) An array of metallic microelectrodes is manufactured by standard MEMS-technology. b) The CNT-dispersion is applied and the solvent allowed to evaporate. c) After the removal of exessive nanotubes, CNTs can only be found in the electrodes cavity.

2.1.2. Gold-Nanowires

Gold nanowires can be integrated by either seed mediated growth [21] or electrodepositioning gold into a template such as aluminum oxide [9] or track etched polycarbonate (PC) membranes [22]. The manufacturing process applied here is described in detail in [10] and depicted in Figure 2. In short a track etched PC-membrane is thermally laminated onto a previously structured photoresist and thus integrated into the microsystem (Figure 2a). Gold is subsequently electrodepositioned into the pores of the membrane (Figure 2b), which is finally removed in a solvent (Figure 2c).

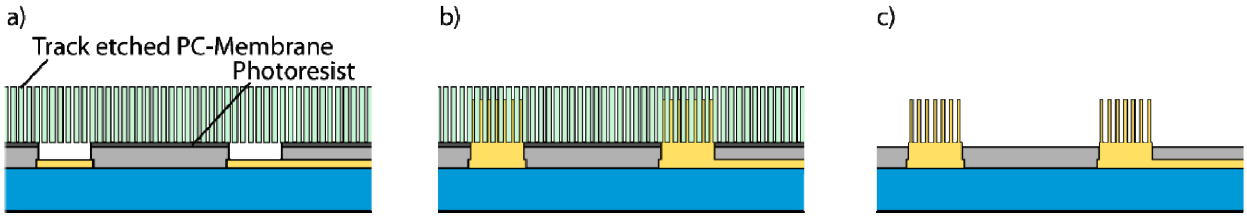

Figure 2. Integration of gold nanowires. a) A track etched PC-membrane is thermally laminated onto a structured thin layer of photoresist. b) the pores are subsequently filled with gold. After removal of the template free standing nanowires are integrated onto the microelectroes.

2.2. Transfer function of the Point-Contact-Model

The interface between a neuron and a microelectrode is modeled by a point-contact model [23] as depicted in Figure 3, where the interface between electrode and electrolyte is modeled by a parallel circuit of the capacitor C_{el} and resistor R_{el}. Similarly, the cell membrane is described by C_m and R_m. Membrane segments that do not participate in the interface are indexed with nm (non-coupling membrane). These C_{nm} and R_{nm} are neglected for further investigations. The ohmic resistance of the electrolyte is represented by R_{spread} and the resistance of the metallic leads by R_{met}. The quality of the cell adhesion can be modeled by the seal-resistance R_{seal}. The closer the coupling the higher is its value. The insulation layer causes a capacity C_{shunt} in the circuit. The voltage is measured between the microelectrode and a reference electrode, which is represented by a R_{ref} - C_{ref} parallel circuit. This impedance however can be neglected because it is very small due to the large size of the reference electrode. Finally the used amplifier is represented by its input impedance Z_{amp}, which is a R-C parallel circuit (not shown). Since C_{shunt} is in parallel to the amplifier capacity these two capacities can be combined. U_m is the intracellular and U_{out} the measurable voltage.

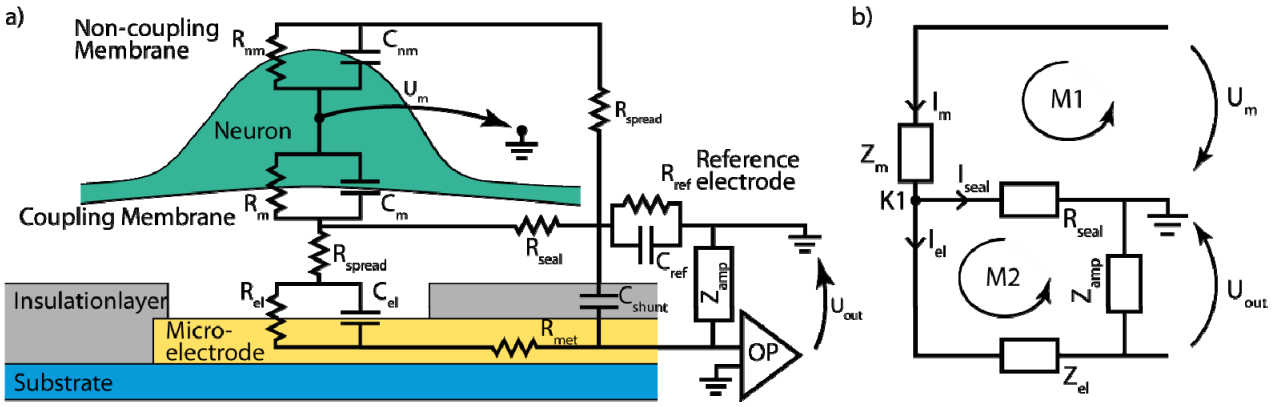

Figure 3. Derivation of the transfer function from the point-contactmodel. a) Point-contact- model of the neuron-electrode interface. All parameters are explained in detail in the text. b)Equivalent circuit derived from the point-contact model of the neuron-electrode interface after simplification. The impedances Z_{amp}, Z_m and Z_{el} are given in Equations 1-3. For clarification the two meshes M1 and M2 and the knot K1 are marked, as well as some specific currents and voltages.

With these considerations and the impedances Z_{amp}, Z_m and Z_{el} given in Equations 1–3 a simplified equivalent circuit (see Figure 3b) is evolved from the complex point-contact-model in Figure 3a.

$$Z_{amp}(j\omega) = \frac{R_{op}}{1+j\omega\, C_{shunt}\, R_{op}} \quad (1)$$

$$Z_m(j\omega) = \frac{R_m}{1+j\omega\, C_m\, R_m} \quad (2)$$

$$Z_{el}(j\omega) = \frac{R_{el}}{1+j\omega\, C_{el}\, R_{el}} + R_{spread} + R_{met} \quad (3)$$

From this simplified equivalent circuit the following equations can be derived [24,25,26]. Here Equations 4 and 5 describe the relationship between voltage and current applying the respective impedance. Equation 6 and 7 are extracted from mesh M1 and mesh M2 respectively. Finally Equation 8 is the knot equation in K1.

$$U_{seal}(\mathrm{j}\omega) = R_{seal} \cdot I_{\mathrm{seal}}(\mathrm{j}\omega) \quad (4)$$

$$U_{out}(\mathrm{j}\omega) = Z_{amp}(j\omega) \cdot I_{\mathrm{el}}(\mathrm{j}\omega) \quad (5)$$

$$U_m(\mathrm{j}\omega) - U_{seal}(\mathrm{j}\omega) = Z_m(j\omega) \cdot I_{\mathrm{m}}(\mathrm{j}\omega) \quad (6)$$

$$U_{mseal}(\mathrm{j}\omega) - U_{out}(\mathrm{j}\omega) = Z_{el}(j\omega) \cdot I_{\mathrm{el}}(\mathrm{j}\omega) \quad (7)$$

$$I_m(\mathrm{j}\omega) = I_{seal}(j\omega) + I_{\mathrm{el}}(\mathrm{j}\omega) \quad (8)$$

The transfer function H(jω) generally is defined as ratio between input and output voltage, in our case $H(\mathrm{j}\omega) = \frac{U_{out}}{U_m}$. By inserting Equations 1-3 and 4-8, the transfer function can be written as below.

$$H(j\omega) = \frac{Z_{amp} R_{seal}}{(R_{seal} + Z_m)(Z_{amp} + Z_{el}) + R_{seal}\, Z_m} \quad (9)$$

If typical values from literature are inserted into these equations the transfer function can be depicted in the form of a bode plot as shown in Figure 4. Here the following values were used [25,26,27]: C_m = 293 pF, R_m = 34 MΩ, C_{el} = 1,14 nF, R_{el} = 140 kΩ, R_{ms} = 12 kΩ, R_{seal} = 1 MΩ, C_{shunt} = 20 pF and R_{op} = 100 GΩ.

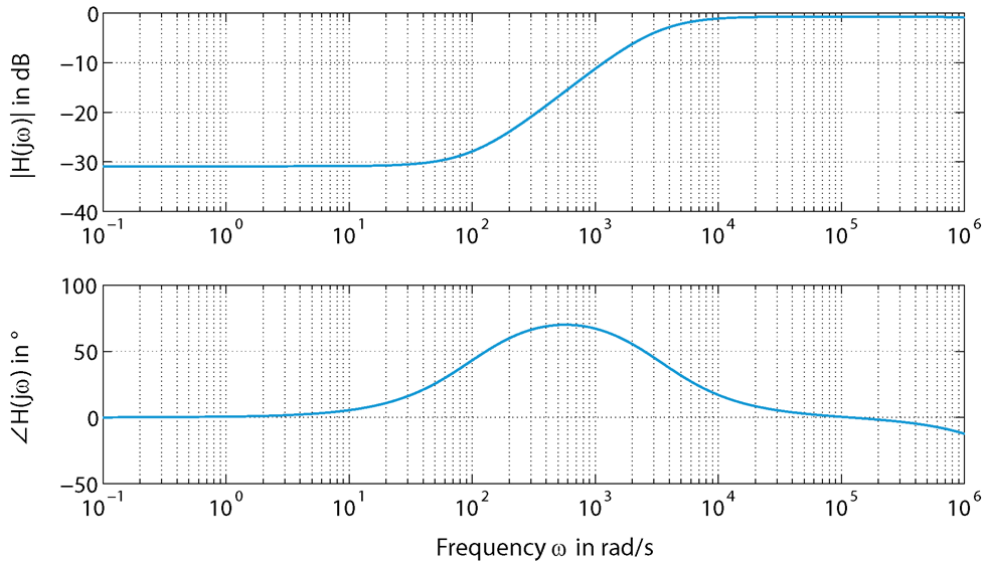

Figure 4. Bode plot of the electrode-neuron transfer function H(jω) according to Equation 6 with typical values taken from literature: C_m = 293 pF, R_m = 34 MΩ, C_{el} = 1,14 nF, R_{el} = 140 kΩ, R_{ms} = 12kΩ, R_{seal} = 1 MΩ, C_{shunt} = 20 pF and R_{op} = 100 GΩ.

Because parameters like the electrode properties C_{el} and R_{el}, the amplifier impedance Z_{amp} or

the capacity C_{shunt} only have a minor effect on the transfer function or can hardly be adjusted in reality like the membrane properties C_m and R_m simulation results are not plotted here. However the transfer function is dramatically influenced by the coupling resistance R_{seal} which is shown in Figure 5.

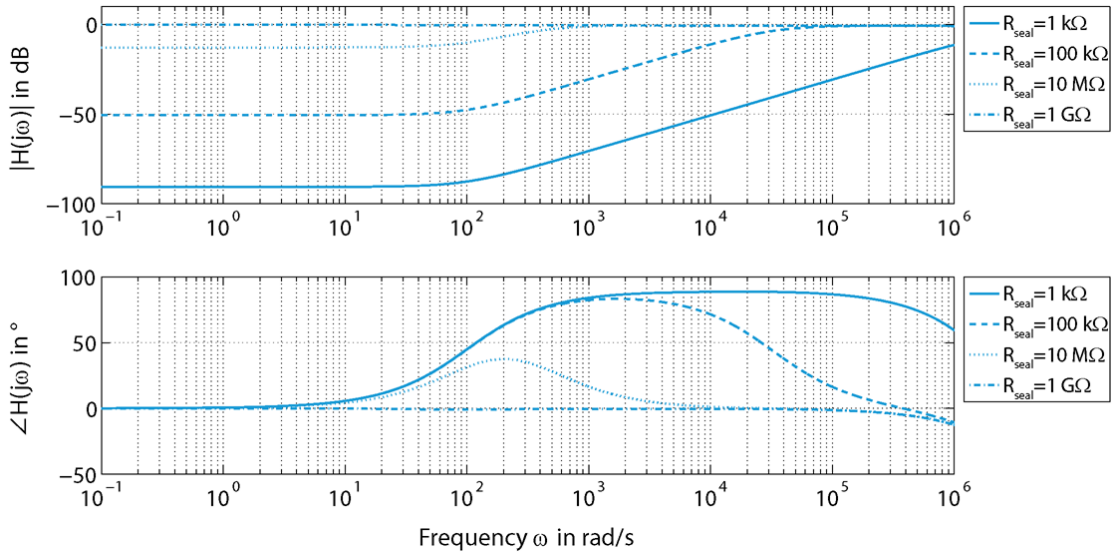

Figure 5. Bode plot of the electrode-neuron transfer function with different values for the coupling resistance R_{seal}. The higher the value the lower is the damping of the signal. This leads to a high measurable signal amplitude at the amplifier.

Obviously the coupling resistance R_{seal} has a great impact on the transfer function as emphasized in Table 1, where magnitude and phase is summarized at the relevant frequency of f = 1 kHz (ω = 6,283 rad/s). This frequency is typically used to evaluate and compare electrode performances because it is within the frequency spectrum of neural activity (800–3,000 Hz) [28].

Table 1. Magnitude and phase of the transfer function for several different values of the coupling resistance R_{seal} at the frequency of 1 kHz.

R_{seal}	1 kΩ	100 kΩ	1 MΩ	10 MΩ	1 GΩ
Magnitude |H(jω)| in dB at f = 1 kHz	−54.77	−14.96	−1.7	−0.66	−0.65
Phase ∠H(jω) in ° at f = 1 kHz	88.39	77.41	26.17	2.31	−0.58

From these results it can be concluded that the measurable signal amplitude can be highly increased by improving the coupling between neuron and electrode. Although the electrode properties itself have only a minor influence on the transfer function, the electrode surface can in fact influence the coupling of a neuron onto the electrode. It has been shown that neurons show a very good coupling to nanostructured surfaces [29,30]. Thus integrating nano objects onto microelectrodes will not only decrease the impedance (see Section 4) and lower the thermal noise but

might also increase the signal amplitude by improving the coupling between cell and electrode.

3. Results

To simulate and predict the behavior of an electrode it is sufficient to focus on the electrodes impedance Z_{el} (see Equation 3). The charge transfer resistance of an electrode, R_{el}, is typically rather large and can be omitted. Thus if only the electrode characteristics are simulated, an even further simplified equivalent circuit of the electrodes capacity C_{el} in series with the two resistors R_{spread} and R_{met}, which are combined as $R_{ms} = R_{spread} + R_{met}$, can be used. Since the impedance determines the thermal noise of the electrode, the effects of integrated carbon nanotubes and gold nanowires shall be studied in the following section. Using the simplified equivalent circuit an electrodes impedance is given by Equation 10 which is a simplification of Equation 3.

$$Z_{el} = R_{ms} + \frac{1}{j\omega C_{el}} \tag{10}$$

Since the capacity is linearly increasing with surface area, the impedance is reduced by the integration of nano objects.

3.1. Electrodes with Integrated Carbon Nanotubes

Carbon nanotubes are tubes of two-dimensional graphene with extraordinary electrical, mechanical and chemical properties. By integrating these nano objects onto microelectrodes the electrochemically active surface area is expected to increase dramatically. To model the properties of electrodes with integrated nanotubes, the expected surface area has to be calculated. Assuming a perfectly cylindrical form the gain in surface area $R_{A,CNT}$ can be calculated with Equation 11. It is assumed that the inside and the outside walls of carbon nanotubes are wetted by electrolyte. If this is not the case the inner diameter r_{in} can be set to 0 and the nanotubes be treated as nanowires.

$$R_{A,CNT} = \frac{n_{CNT} A_{CNT}}{A} + 1 \tag{11}$$

$$R_{A,CNT} = \frac{n_{CNT} 2\pi (r_{out} + r_{in}) l_{CNT}}{A} + 1,$$

where n_{CNT} is the number of carbon nanotubes inside an electrode cavity, A_{CNT} is the total surface area of a single carbon nanotube and A is the geometrical surface of the microelectrode. The number of CNTs inside a cavity can be estimated by the cavities and the CNTs volumes as done in Equation 12. Since not the entire cavity volume is filled with nanotubes, a factor p_{fill} is introduced, representing the ratio of filled volume

$$n_{CNT} = \frac{p_{fill} V_{cavity}}{V_{CNT}} = \frac{p_{fill}\, A\, h_{iso}}{\pi r_{out}^2 l_{CNT}}, \tag{12}$$

with V_{cavity} being the volume of the electrode cavity, V_{CNT} the volume of a single CNT, h_{iso} the height of the insulation layer and l_{CNT} the length of a single nanotube. Inserting Equation 12 into Equation 11 an easy formula to calculate the win of surface area as depicted in Equation 13 is derived

$$R_{A,CNT} = \frac{2\, p_{fill}\, h_{iso}(r_{out}+r_{in})}{r_{out}^2} + 1, \qquad (13)$$

with a typical length of l_{CNT} = 1.5 µm, and radii of r_{out} = 4.25 nm and r_{in} = 3.1 nm [31], a height of h_{iso} = 5 µm and a filling ratio of p_{fill} = 1/3 $R_{A,CNT}$ equals 1,357. Figure 6 depicts the bode plots for a planar gold electrode with C_{el} = 0.1 nF and R_{ms} = 10 kΩ [9] and a CNT electrode with increased capacity. The value for the resistor R_{ms} is kept constant.

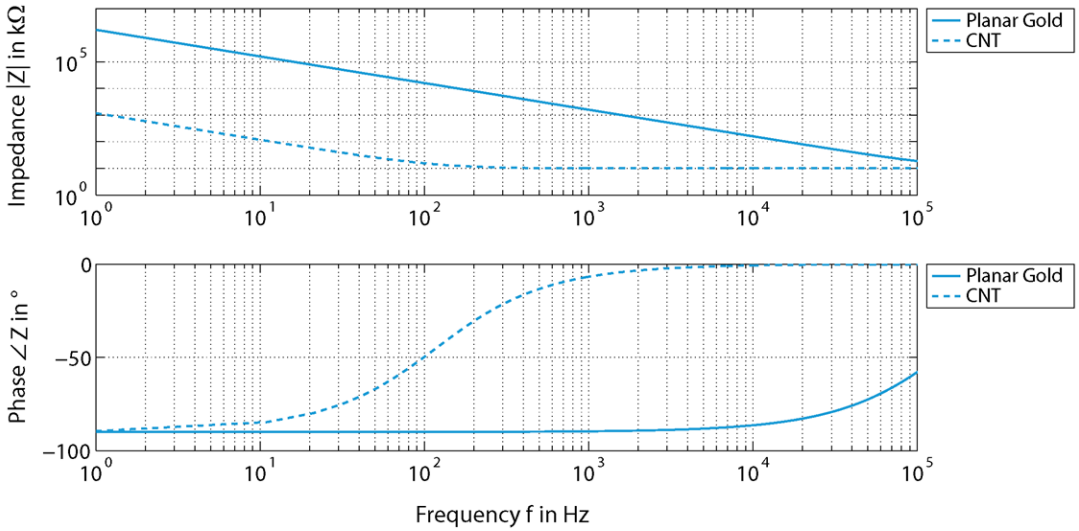

Figure 6. Bode plot for planar gold electrodes and electrodes with integrated carbon nanotubes. Obviously the nanostructures lead to a highly decreased impedance over the entire frequency range. For frequencies higher than approximatly 100 Hz when phase is larger than −45° the resistor dominates the electrodes behavior of CNT electrodes.

Clearly the integration of carbon nanotubes leads to a decrease in electrode impedance over the entire frequency range. For higher frequencies larger than approximately 100 Hz, when phase is larger than −45° the resistor dominates the impedance of CNT electrodes, resulting in a magnitude of approximately 10 kΩ. A phase angle of 0° is approached for frequencies in excess of 10^3 to 10^4 kHz.

3.2. Electrodes with Integrated Gold Nanowires

The noble metal gold is known for its biocompatibility and high corrosion resistivity and thus ideal for this application. Although the material itself has no impact on the simulation, measurements will be done with gold. In contrast to carbon nanotubes metallic nanowires are bulk material and thus only the (outer) surface of the nanowires add to the new overall electrode area. By integrating nanowires into the microsystem the capacity can be increased by increasing the active surface area. The gain in surface area $R_{A,AuNW}$ in this case depends on the height of the wires

$$R_{A,AuNW} = 2\,\pi\, r_{AuNW}\, h_{AuNW} \rho_{AuNW} + 1, \qquad (14)$$

where r_{AuNW} is the radius of a gold nanowire, h_{AuNW} is its height and ρ_{AuNW} the nano wire density. Assuming a density of ρ_{AuNW} = 6 µm^{-2}, a radius of r_{AuNW} = 100 nm and a planar capacity of C_0 the

electrodes capacity can be calculated according to $C = (3.77\ h_{AuNW}/\mu m + 1)\ C_0$. If the planar capacity is again set to $C_0 = 0.1$ nF and the resistor to $R_{ms} = 10$ kΩ the height depended electrodes properties summarized in Table 2 and depicted in Figure 7 are obtained.

Table 2. Magnitude and phase of an electrodes with integrated gold nanowires for several different heights at the frequency of 1 kHz.

h_{AuNW}	0 µm	5 µm	10 µm	15 µm	25 µm
Magnitude |Z(jω)| in kΩ at f = 1 kHz	1592	81	42	29	19
Phase ∠Z(jω) in ° at f = 1 kHz	−90	−83	−76	−70	−59

As expected the higher the nanowires are, the lower the impedance is. By integrating gold nanowires the impedance can be decreased for the entire frequency range.

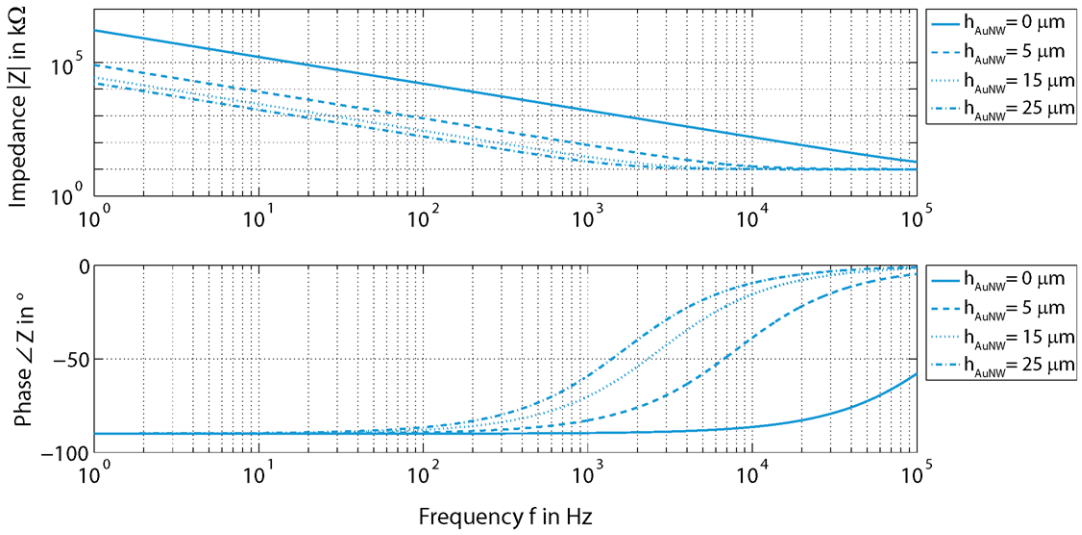

Figure 7. Bode plot for a planar gold electrode and electrodes with integrated gold nanowires with different heights. By integrating gold nanowires the impedance can be decreased over the entire frequency range. As expected the heights h_{AuNW} has a strong influence on the impedance spectra.

4. Discussion

To evaluate the simulated electrode properties with experimental findings microelectrodes are manufactured and characterized by cyclic voltammetry and electrochemical impedance spectroscopy. All measurements are done with electrolyte phosphate buffered saline (PBS, Sigma Aldrich). Cyclic voltammetry is performed in a three-electrode set-up, using the microelectrodes as working electrodes, a platinum mesh as counter electrode and an Ag/AgCl electrode as reference. From the resulting U-I-diagrams (not shown) the DC-capacity is evaluated [20]. Impedance spectroscopy is performed in a frequency range of 1 Hz–100 kHz to cover the entire neuronal frequency spectrum and beyond. The manufactured microelectrodes serve as working electrodes and an Ag/AgCl pellet electrode

(Multichannel Systems, Reutlingen, Germany) as combined counter/reference electrode. Furthermore the impedance data can be fitted with an equivalent circuit to extract the AC-properties of the electrode such as capacity and resistance. Due to ion idleness in AC-conditions not the entire surface is effective at the interface and the AC-capacity is expected to be smaller than the DC-capacity.

4.1. Electrodes with Integrated Carbon Nanotubes

With cyclic voltammetry a capacity gain between a planar gold electrode and an electrode with integrated carbon nanotubes is measured to 1,800. This value is somewhat higher than the expected factor of 1,357. The discrepancy can be explained by slight deviations in electrode size due to the manufacturing process.

When observing the AC-properties of the electrode it becomes obvious that under these circumstances not the entire surface contributes to the electrochemical interface, which results in a reduced capacity. Ions are not able to follow the alternating electric field into the pores, eliminating some of the effective capacity. This effect causes the impedance to decrease only by a factor of 62 and not as expected by a factor of 158. Measured impedance spectra for a planar gold electrode and an electrode with carbon nanotubes are depicted in Figure 8. The fundamental shape is in good agreement with the theoretical properties (see Figure 6). It can be seen that the resistor is dominating at a frequency of about 2000 Hz since the capacity is nearly short circuited at this frequency. From simulations this was expected to happen already at about 200 Hz. Reason for this discrepancy could be that not the entire surface area contributes to the electrochemical interface in AC-conditions.

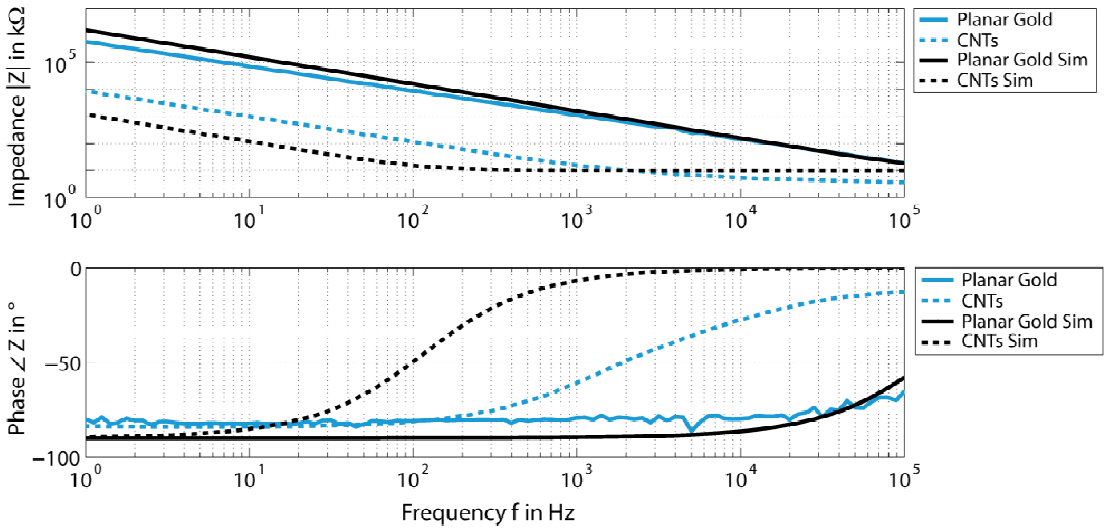

Figure 8. Meassured impedance spectra of manufacutred 30 µm-microelectrodes with planar gold and integrated carbon nanotubes in comparison to simulated data from Figure 6. The measurements (blue lines) are generally in good agreement with the simulated data (black lines).

4.2. Electrodes with Integrated Gold Nanowires

For microelectrodes with integrated gold nanowires a DC-capacity linearly dependent on the height is revealed in cyclic voltammetry as shown in Table 3. This table also summarizes the AC-properties revealed by electrochemical impedance spectroscopy which are also shown in Figure 9. The measured impedance spectra are in good agreement with the simulated electrode properties. If the ratios are calculated for 20.4 µm nanowires the DC-capacity increases by a factor of 90 and the impedance is decreased by a factor of 109.

Table 3. DC-capacity, magnitude and phase of an 30 µm-electrode for several different heights of integrated gold nanowires. Capacity is increasing with height which causes the impedance to decrease.

h_{AuNW}	**0 µm**	**5.2 µm**	**10.7 µm**	**20.4 µm**
DC-capacity C_{DC} in mF/cm^2	0.035± 0.028	0.66 ± 0.24	1.61 ± 0.83	3.17 ± 1.04
Magnitude |Z(jω)| in dB at f = 1 kHz	1585 ± 141	121 ± 46	53.83 ± 9.03	14.5 ± 2.6
Phase ∠Z(jω) in ° at f = 1 kHz	−84.32 ± 0.58	−79.44 ± 2.03	−75.57 ± 2.03	−66.60 ± 2.00

Because the DC-capacity and impedance at 1 kHz are influenced by similar factors it can be concluded that the interspaces between gold nanowires are wide enough that ions are able to follow even an alternating field. Thus the entire surface area is contributing to the electrochemical interface.

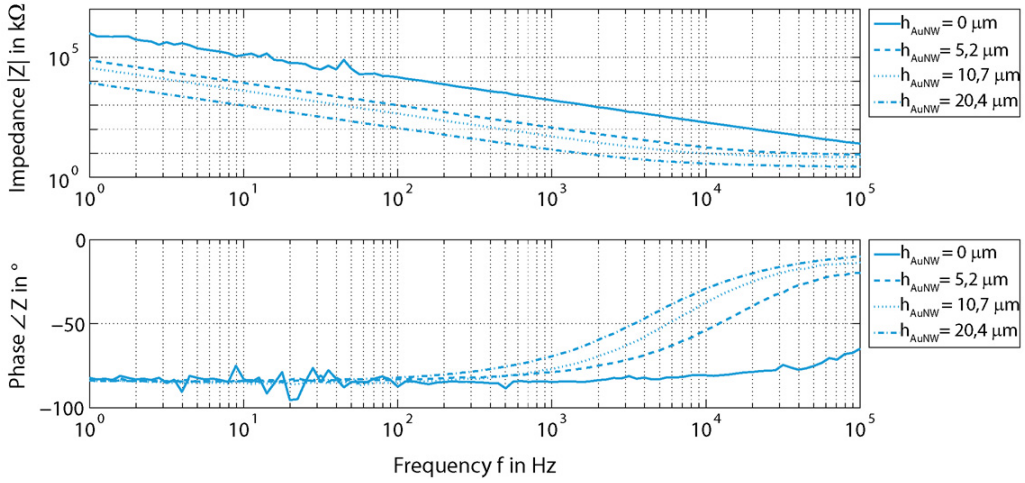

Figure 9. Meassured impedance spectra of manufacutred 30 µm-microelectrodes with planar gold and integrated gold nanowires with several heights. These measurements are in very good agreement with the simulated data (see Figure 7).

Figure 10 shows the simulated and measured magnitude and phase at 1 kHz plotted against the height of gold nanowires. From about 15 µm onwards the impedance is not reduced much further. This is due to the large capacity that it is nearly short-circuited at 1 kHz. Consequently the impedance is dominated by the resistor R_{ms}. The measured results are in very good agreement to the simulated data.

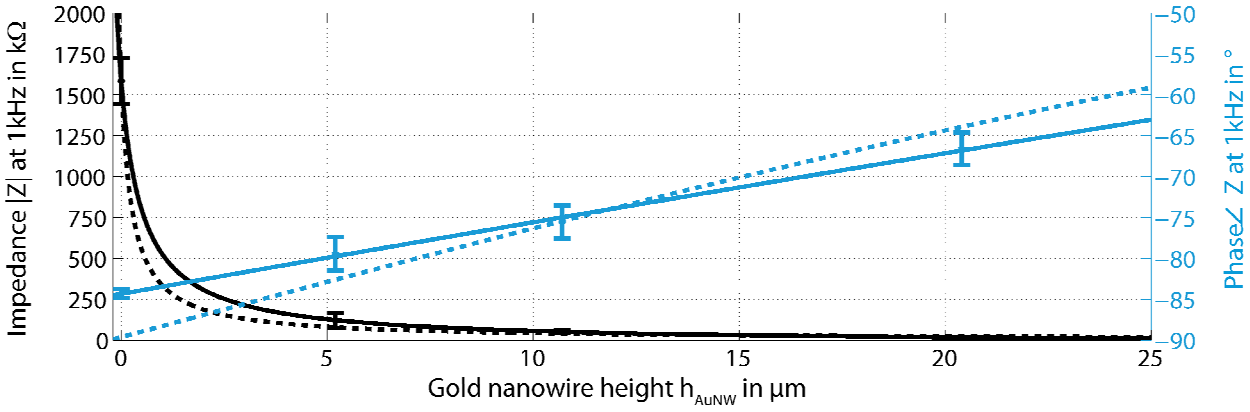

Figure 10. Height dependence of the impedances magnitude and phase at 1 kHz simulated (dotted lines) and measured (line) with manufactured 30 µm-microelectrodes. Simulation and measurements are in good agreement.

5. Conclusion

For recording electrodes in the nervous system a high signal-to-noise ratio is desired. In this work we present a transfer function defined as ratio between the membrane potential of neuron and an extracellular microelectrode. The influence of relevant parameters was studied to find that the coupling resistance R_{seal} has a great effect on the function. This resistance can be increased by an improved adhesion between cell and electrode, resulting in low losses and thus an increase in signal amplitude. To further increase the SNR not only the recorded signal amplitude should be increased but also the noise should be decreased at the same time. Since noise is dominantly thermal, this can be achieved by decreasing the electrodes impedance by increasing the electrochemical active surface area through the integration of different nano structures. The influence of the integration of carbon nanotubes and gold nanowires onto the electrodes behavior (impedance) was simulated and measured with manufactured electrodes.

By increasing the coupling resistance R_{seal} and decreasing the impedance, the integration of nano objects onto microelectrodes has the potential to significantly improve the signal-to-noise ratio of neuroelectrodes. Here simulations of electrode properties are compared with experimental findings. Electrodes with integrated carbon nanotubes show a DC-capacity that is 1,800-fold higher compared to a planar gold electrode which is in good agreement to simulations. The AC-impedance however at 1 kHz is only reduced by a factor of 62 which is less than the expected value. Ions are not able to follow the alternating electric field into the pores, reducing the effective capacity. Electrodes with integrated gold nanowires show height dependent DC- and AC-properties that are in good agreement with simulation results.

Acknowledgments

C.N. expresses his gratitude for the Studienstiftung des Deutschen Volkes for supporting his research.

Conflict of Interest

The author declares no conflicts of interest in this paper.

References

1. Wilson B, Dorman M (2008) Cochlear implants: A remarkable past and a brilliant future. *Hearing Res* 242: 3–21.
2. Zrenner E (2013) Fighting Blindness with Microelectronics. *Sci Transl Med* 5(210): 210ps16.
3. Perlmutter J, Mink J (2006) Deep brain stimulation. *Annu Rev Neurosci* 29: 229–257.
4. Priori A, Foffani G, Rossi L, et al. (2012) Adaptive deep brain stimulation (aDBS) controlled by local field potential oscillations. *Exp Neurol* 245: 77–86.
5. Gallentine W, Mikati M (2009) Intraoperative electrocorticography and cortical stimulation in children. *J Clin Neurophysiol* 26: 95–108.
6. Keefer E, Botterman B, Romero M, et al. (2008) Carbon nanotube coating improves neuronal recordings. *Nat Nanotechnol* 3: 434–439.
7. Ben-Jacob E, Hanein Y (2008) Carbon nanotube micro-electrodes for neuronal interfacing. *J Mater Chem* 18: 5181–5186.
8. Nick C, Joshi R, Schneider J, et al. (2012) Three-dimensional carbon nanotube electrodes for extracellular recording of cardiac myocytes. *Biointerphases* 7: 58–64.
9. Brüggemann D, Wolfrum B, Maybeck V, et al. (2011) Nanostructured gold microelectrodes for extracellular recording from electrogenic cells. *Nanotechnology* 22: 265104.
10. Nick C, Quednau S, Sarwar R, et al. (2014) High Aspect Ratio Gold Nanopillars on Microelectrodes for Neural Interfaces. *Microsyst Technol* 20: 1849–1857.
11. Kim D, Abidian M, Martin D (2004) Conducting Polymers Grown in Hydrogel Scaffolds Coated on Neural Prosthetic Devices. *J Biomed Mater Res A* 71: 577–585.
12. Poppendieck W, Hoffmann K-P (2009) In 4th European Conference of the International Federation for Medical and Biological Engineering Springer: 2409–2412.
13. Potter S, DeMarse T (2001) A new approach to neural cell culture for long-term studies. *J Neurosci Methods* 110: 17–24.
14. Potter S (2001) Distributed processing in cultured neuronal networks In M.A.L. Nicoleleis, (ed.), Advances in Neural Population Coding (Progress in Brain Research), 130: 49–62.
15. Hoogerwerf A, Wise K (1994) A Three-Dimensional Microelectrode Array for Chronic Neural Recording. *IEEE Trans Biomed Eng* 41: 1136–1146.
16. Nordhausen C, Maynard E, Normann R (1996) Single unit recording capabilities of a 100 microelectrode array. *Brain Res* 726: 129–140.
17. Gabay T, Ben-David M, Kalifa I, et al. (2007) Electro-chemical and biological properties of carbon nanotube based multi-electrode arrays. *Nanotechnology* 18: 035201–035206.

18. Fuchsberger K, Le Goff A, Gerwig R, et al. (2010) Integration of Carbon Nanotubes in Microelectrode Arrays by Microcontact Printing and Electropolymerization for Neurostimulation and Biosensing Applications. In 7th Meeting on Substrate-Integrated Microelectrodes, Reutlingen, Germany; 267–268.
19. Gabriel G, Gomez-Martinez R, Villa R (2008) Single walled carbon nanotubes deposited on surface electrodes to improve interface impedance. *Physiol Meas* 29: 203–212.
20. Nick C, Thielemann C (2014) Are Carbon Nanotube Microelectrodes Manufactured from Dispersion Stable Enough for Neural Interfaces? *Bio Nano Sci* 4: 216–225.
21. Bauer L, Birenbaum N, Meyer G (2004) Biological applications of high aspect ratio nanoparticles. *J Mater Chem* 14: 517–526.
22. Wang H-W, Shieh C-F, Chen H-Y, et al. (2006) Standing [111] gold nanotube to nanorod arrays via template growth. *Nanotechnology* 17: 2689–2694.
23. Pancrazio J, Whelan J, Borkholder D, et al. (1999) Development and application of cell-based biosensors. *Ann Biomed Eng* 27: 697–711.
24. Joye N, Schmid A, Leblebici Y (2008) An electrical model of the cell-electrode interface for high-density microelectrode arrays. In Proceedings of the 30th Annual International Conference of the IEEE Engineering in Medicine and Biology Society: 559–562.
25. Sessler F, Hsu F, Felder T, et al. (1998) Effects of ethanol on rat so mato sensory cortical neurons. *Brain Res* 804: 266–274.
26. Massobrio P, Massobrio G, Martinoia S (2007) Multi-program approach for simulating recorded extracellular signals generated by neurons coupled to microelectrode arrays. *Neurocomputing* 70: 2467–2476.
27. Gabay T (2009) Carbon Nanotube Microelectrode Arrays for Neuronal Patterning and Recording (PhD thesis) Tel-Aviv University.
28. Bauerdick S, Burkhardt C, Kern D, et al. (2003) Substrate-Integrated Microelectodes with Improved Charge Transfer Capacity by 3-Dimensional Micro-Fabrication. *Biomed Microdevices* 5: 93–99.
29. Sorkin R, Gabay T, Blinder P, et al. (2006) Compact self-wiring in cultured neural networks. *J Neural Eng* 3: 95–101.
30. Sorkin R, Greenbaum A, David-Pur M, et al. (2009) Process entanglement as a neuronal anchorage mechanism to rough surfaces. *Nanotechnology* 20: 015101.
31. CNT Expertise Centre (2009) Available from: http://www.nanocyl.com/en/CNT-Expertise-Centre/Carbon-Nanotubes.

AIMS Press